Simultaneously enhanced photocatalytic and antibacterial activities of TiO_2/Ag composite nanofibers for wastewater purification

Lei Wang [†, a], Jafar Ali [†, a, c], Changbo Zhang [*, b], Gilles Mailhot [*, d] and Gang Pan [*, a, e]

[a] Department of Environmental Nanotechnology, Research Center for Eco-environmental Sciences, Chinese Academy of Sciences, 18 Shuangqing Road, Beijing 100085, P. R. China.

[b] Agro-Environmental Protection Institute, Ministry of Agriculture, Tianjin 300191, P. R. China.

[c] University of Chinese Academy of Sciences, Beijing 100049,China

[d]Institut de Chimie de Clermont-Ferrand, Université Clermont Auvergne, CNRS, SIGMA Clermont, 24 avenue des Landais, Aubière, France

[e] School of Animal, Rural and Environmental Sciences, Nottingham Trent University, Brackenhurst Campus, Southwell NG25 0QF, United Kingdom

† Co-first author with the same contribution to this work.

* Corresponding authors: gpan@rcees.ac.cn (Gang Pan), zhchb1976@163.com (Changbo Zhang) and gilles.mailhot@uca.fr (Gilles Mailhot)

Abstract

High throughput of polyacylonitile (PAN)-based Ag/TiO_2 composite nanofibers were prepared by using needleless electrospinning method. The morphology and crystallinity characterization revealed uniform and smooth nanofibers with an average diameter ranged from 160 to 260 nm. The enhanced photocatalytic activity of PAN/Ag/TiO_2 compared with PAN/TiO_2 nanofibers under visible light irradiation was linked with high interfacial charge transfer and low bandgap due to Ag entity. High photodegradation efficiency for methyl orange, rhodamine B and methylene blue were achieved as 99.5%, 92% and 99% respectively during the 4 h experiment. Effect of key parameters (i.e. pH, oxygen and Ag/TiO_2 loading dosage) on photodegradation efficiency of dyes were also investigated. Active species trapping experiments demonstrated that •O_2- and •OH were dominant active species in the photocatalytic degradation of dyes. These composite nanofibers have also exhibited excellent antibacterial activity, e.g. 95% of *E. coli* and 99% of *S. aureus* were killed in 2 h. Bifunctional nanofibers can be easily recovered from the aqueous solution as compared with the TiO_2 nanoparticles. Moreover, the daily production rate of nanofibers has reached over 1.4 kg in the laboratory test, which is 60 times higher than that using the single needle electrospinning method. This production rate may be further optimized in the pilot scale studies. High productivity and strong catalytic properties of nanofibers propose their potential applications in environmental remediation for economically and eco-friendly wastewater and air treatment materials.

Keywords: TiO_2 nanofiber; Wastewater treatment; Ag nanoparticles; Photocatalytic

degradation; Antibacterial activity; Dye pollutants

Introduction

Titanium dioxide (TiO_2) nanoparticles have been extensively used in the environmental applications such as wastewater purification as well as solar energy conversion owing to their exceptional oxidizing power, non-toxicity and long-term photo-stability [1-4]. However, wide band gaps and charge carrier recombination are some intrinsic drawbacks of titanium dioxide (TiO_2) nanoparticles, which limits their photocatalytic efficiency and broader applications [5]. Moreover, immobilization of TiO_2 based catalysts on various supporting matrices for reuse in photocatalytic membrane reactors have also been studied [6, 7]. Conversely, immobilization has resulted in high cost and reduction of removal efficiencies of organic pollutants due to substantial loss of photocatalytic active surface area. Therefore, it is highly desired to develop the cost effective, immobilized TiO_2 nanomaterials with enhanced photocatalytic activity and high surface area. Various strategies have been employed to increase photocatalytic activity, such as impurity doping [8, 9], surface fluorination [10], and noble metal deposition [11-13].

Interestingly, silver doped TiO_2 materials can enhance the electron-hole separation and interfacial charge transfer, eventually increasing the photocatalytic activity along with extending the working area to the visible light region [14, 15]. Moreover, silver doped TiO_2 matrix has many other implications ranging from antimicrobial material [16, 17], humidity sensor [18], and photocatalyst [19]. Recently, nanofibers have been proved as an efficient heterogeneous photocatalysts and useful supporting matrix for

catalytic metal nanoparticles [20-23]. Electrospinning offers a simple and versatile method to produce various binary or multicomponent nanocomposites via sol-gel processes [24-26]. Numerous composite nanofibers can be fabricated by varying the composition of the electrospinning solutions containing two or more soluble precursors. However, few researchers have tried the combination of TiO_2 and silver nanoparticles (AgNPs) in a polymeric matrix to enhance their synergistic effects and characteristics such as mechanical, optical, photocatalytic, and antimicrobial properties [27-29].

Similarly, studies focusing on improving the productivity of Ag/TiO_2 composite nanofibers are less reported, thus limiting the potential applications of hybrid nanofibers in the pilot scale context and commercial scale. However, a majority of researchers are using two separate steps for the decoration of TiO_2 and AgNPs on polymeric nanofibers surfaces. Conclusively, aforementioned synthesis approaches are complicated, expensive and not efficient [22, 30, 31]. Hence, there is still need to explore some innovative strategies for the production of novel composite nanofibers with diverse implications. In this study, we have reported, the facile, high throughput synthesis of PAN-based Ag/TiO_2 composite nanofibers using needleless electrospinning method. The daily productivity of nanofibers was quantified to compare the efficiency of our method. Our one-step electrospinning method features the novelty of using electrospinning solvent N, N-dimethylformamide (DMF) as a reducing agent for the in situ synthesis of AgNPs [32].

The photocatalytic activity of $PAN/Ag/TiO_2$ composite nanofibers ($PAN/Ag/TiO_2$

NF) was measured by degradation of dye pollutants. Meanwhile, factors affecting the photo degradation efficiency, such as the loading dosage of Ag and TiO_2, initial pH and oxygen were also evaluated. In addition, underlying degradation mechanism was explored by probing the active species trapping experiments. Experimental results have demonstrated that the PAN/Ag/TiO_2 NF were simultaneously efficient as a photocatalyst and antimicrobial agent. These findings may offer the potential applications in the field of photocatalysis, sterilization and environment purification.

2. Materials and methods

2.1. Materials

Polyacrylonitrile (PAN, Mw = 150k) was purchased from Aldrich. N, N-dimethylformamide (DMF) and $AgNO_3$ were obtained from Beijing Chemical Works (Beijing, China). TiO_2 (Anatase, particle size of 5-10 nm) was obtained from Evonik Industries Metal Oxides. Ethylenediaminetetraacetic acid (EDTA), benzoquinone (BQ) and tertiary butyl alcohol (TBA) were purchased from Aladdin (China). All chemicals were used without further purification. Water was obtained from a Milli-Q system (Millipore Corp., Boston, MA).

2.2. Preparation of PAN/Ag/TiO_2 composite nanofibers

A 10 wt% solution of PAN in DMF was prepared by stirring the polymer and solvent at 50 °C for 24 h to obtain a viscous and transparent polymer solution. Different concentrations of TiO_2 and $AgNO_3$ were dispersed in this PAN/DMF solution by stirring and the mixture was sonicated in order to ensure good dispersal. When reaction mixture was cooled down to the room temperature, it was placed into a

polytetrauoroethylene solution tank. Then the needleless electrospinning setup was used as described in our previous work [33]. The electrospinning experiments were carried out at 25 °C, relative humidity of 20%, applied voltage of 50 kV, distance from the tank to the collector (TCD: 15 cm), the rotation speed of spinning electrode and collector was 20 rpm and 50 rpm, respectively. The nanofiber mats were collected on a grounded roller and subsequently dried at room temperature in vacuum for 24 h.

2.3. Characterization of nanofibers

The morphology and composition of the samples were characterized by scanning electron microscopy (SEM, S4800, HITACHI), transmission electron microscopy (TEM, Tecnai G2 20 S-TWIN, FEI), energy dispersive X-ray spectroscopy (EDX, Horiba), X-ray diffraction (XRD, Regaku D/Max-2500 diffractometer equipped with a Cu $K\alpha_1$ radiation) and UV-Vis absorption spectrometer (Shimadzu UV-3101 Spectrometer). The conductivity of the electrospinning solution was determined by the conductivity meter (DDS-11A, Shanghai REX Instrument Factory). The average diameter of nanofiber was determined by a statistical analysis of the SEM image with an image processing software Image J.

2.4. Photocatalytic activity

Photocatalytic activities of PAN/Ag/TiO_2 NF were investigated by perceiving degradation of methyl orange, rhodamine B and methylene blue under 250 W metal halide lamp with the major emission wavelengths above 400 nm (Shanghai Yaming Light, China). The light was filtered by the cutoff filter (>420 nm) to simulate the visible light. 100 mL of 10 ppm dyes solution was added to a beaker and

PAN/Ag/TiO_2 or PAN/TiO_2 electrospun mats of size 4×4 cm^2 were put into the solutions with concentration of 50 ppm. The lamp was then turned on to allow photocatalytic reaction. Dyes concentrations were measured from UV–vis spectra of sampling aliquots subsequently removed (at different intervals) using UV–vis spectrophotometer (Shimadzu UV-3101 Spectrometer). The photocatalytic removal efficiency (R) of dyes were calculated by the following equation:

$$R = (1 - C/C_0) \times 100\%$$

Where C_0 was the initial concentration and C_t was the concentration at various irradiation time.

The photocatalytic activity of PAN/Ag/TiO_2 composite nanofibers were tested by decoloring the dye stains on the membrane.

In order to investigate the possible photocatalytic mechanism, active species trapping experiments were conducted with different scavengers. Benzoquinone (BQ, 1 mM), tertiary butyl alcohol (TBA, 1 mM) and EDTA (1 mM) were used as scavengers for trapping superoxide radical ($\bullet O_2^-$), hydroxyl radicals (•OH) and holes (h^+), respectively [34]. The experimental conditions were kept the same to the aforementioned photodegradation experiment. All the experiments were performed in triplicate.

2.5. Testing of antibacterial activity

The antibacterial properties of PAN/Ag/TiO_2 nanofibers mats against *Escherichia coli* (ATCC 25922) and *Staphylococcus aureus* (ATCC 6538P) were tested by agar plate method. Nanofiber samples were first cut into wafers with diameter of 1cm and

these wafers were treated with ultraviolet radiation for 30 min. After the activation, bacteria were inoculated and cultured on nutrient agar plate at 37 °C. The prepared nanofiber samples were placed onto the substrates. The plates were incubated at 37 °C for 24 h. Images of the plates were taken to illustrate the antibacterial performance of the samples.

The shake flask method was used to examine the bactericidal kinetics of the electrospun PAN/Ag/TiO_2 composite nanofibers. Non-woven mats of PAN/Ag/TiO_2 were added into tubes containing the test bacteria at a concentration of 7×10^6 CFU/mL in the Difco Nutrient Broth solution. The tubes were incubated in shaking incubator at 37 °C. Samples of the non-woven mats of PAN/Ag/TiO_2 blends with the same weight and size (5 mg and 4 cm×4 cm) were used. Aliquots (0.1 mL) of the solution were sampled and quickly spread on a plate containing nutrient agar after every half hour. The plates with bacterial cultures were also incubated at 37 °C for 24 h and the bacterial colonies were counted.

3. Results and Discussion

3.1. Preparation and characterization of Ag/TiO_2 composite nanofibers

The needleless electrospinning method was used to prepare the PAN-based Ag/TiO_2 composite nanofibers. The generation rate of nanofibers by needleless electrospinning method was 60.0 g h^{-1}, while the nanofibers generation rate by single needle electrospinning method was only 0.02-1.0 g h^{-1}. Needleless electrospinning method has significantly improved the production rate of nanofibers, which is about 60 times higher than the single needle electrospinning method. The SEM images of

PAN-based electrospun nanofiber mats containing 2 wt% TiO_2 and 5 wt% $AgNO_3$ are shown in Fig. 1a. PAN/Ag/TiO_2 composite nanofibers present neat and uniform morphology with average diameter of 208 nm (Fig. 1b). The $AgNO_3$ addition considerably improved the spinning ability of the mixed solutions to form uniform functional nanofibers. The distribution of TiO_2 and AgNPs in the PAN/Ag/TiO_2 composite nanofibers was characterized by TEM (Fig. 1c) where, Ag and TiO_2 NPs were uniformly dispersed across the entire nanofiber matrix. Fig. 1d shows the EDX spectra of the nanofibers. The peaks of elemental Ag and Ti were the additional evidence for the formation of AgNPs and TiO_2 on the surface of the nanofibers.

Effect of various concentrations of $AgNO_3$ and TiO_2 were also investigated in this work. The PAN/Ag/TiO_2 hybrid nanofibers were obtained with smooth and uniform morphology and the average diameter was in the range of 160-260 nm (table 1). When TiO_2 concentration was increased, the diameter of composite nanofibers was slightly decreased. The reduction in diameter can be attributed to TiO_2 because it relatively increases the viscosity than conductivity of the spinning solution at the time of formation of nanofibers. The diameters of nanofibers were decreased with the increase in $AgNO_3$ concentration. From table 1, at higher $AgNO_3$ concentration the conductivity was higher and the electrospun filament was further attenuated by the electric field during the electrospinning process.

3.2. XRD analysis

The XRD patterns of PAN hybrid nanofibers without and with TiO_2/AgNPs are displayed in Fig. 2. The XRD pattern of the pure PAN nanofibers showed diffraction

peak of carbon at a 2θ value of 23.5 and a broad noncrystalline peak at about 16-20. In the XRD pattern of PAN nanofibers containing TiO_2, these peaks appeared at 2θ values of 25.32, 37.86, 48.06, 53.97, 55.09 and 62.75, which were corresponded to the diffraction peaks of anatase TiO_2 (101), (004), (200), (105), (211) and (204). In the PAN/Ag/TiO_2 composite mats, the characteristic peaks appeared at 2θ values of 38.12, 44.28, 64.43 and 77.47, corresponding to the crystal planes (111), (200), (220), and (311) indicating the presence of AgNPs in composite mats. These values are in agreements with the International Center for Diffraction Data (ICDD) card (card no.4-783).

3.3. UV–vis spectra of composite nanofibers

Fig. 3 is depicting the absorption spectra of PAN hybrid nanofibers containing 2 wt% TiO_2 and 5 wt% $AgNO_3$. The wavelength distribution of the absorbed light is a vital property of photocatalyst, which is corresponding to the region of utilized light. As shown in Fig. 3, the absorption curve of PAN/TiO_2 nanofiber mats was clearly different from that of PAN/Ag/TiO_2 composite nanofibers. The peaks observed around 450-530 nm could be ascribed to the surface plasmon absorption of spatially confined electrons in AgNPs [35, 36]. The absorptive edge of PAN/Ag/TiO_2 composite nanofibers is manifested an obvious red-shift towards longer wavelengths, thus broad and intense absorption covered nearly the whole visible region. The unique absorptive characteristics would be attributed to the marked quantity of AgNPs, which have contributed mainly to decrease the band gap of TiO_2. This red-shift might be related to the high refractive index of the TiO_2 matrix and/or interaction between

AgNPs and TiO_2 [37].

3.4. Photocatalytic activity of PAN/Ag/TiO_2 composite nanofibers

The photocatalytic activity of the PAN/Ag/TiO_2 composite nanofibers was investigated by photocatalytic degradation of different dye solutions with methyl orange, rhodamine B and methylene blue. Evidently, there was almost no photodegradation of dyes without nanofibers (Fig. 4), which was indicating negligible photo induced self-decomposition of these pollutants. However, under the dark conditions absorption efficiency of dyes were about 17.0%, 19.0% and 6.0% for methyl orange, rhodamine B and methylene blue, respectively. As shown in Fig. 4, the photocatalytic degradation rates of dyes in the presence of the PAN/Ag/TiO_2 NF were apparently higher than that of PAN/TiO_2 NF. Fig. 5 showed the absorbance of dyes solution according to the irradiation time in the presence of PAN/Ag/TiO_2 NF. These findings clearly showed that AgNPs modified nanofibers could enhance the photocatalytic properties of TiO_2. Perhaps AgNPs have worked as a sink for electrons on the surface of TiO_2, which have contributed to the interfacial charge transfer between the metal and semiconductor as well as separation of photogenerated electron-hole pairs, eventually enhancing the photocatalytic activity. After reaction, these composite nanofibers were much more easily recovered from the reaction solution as compared with the TiO_2 nanoparticles.

Different parameters influencing the photodegradation of dyes solution were also investigated in current work. As shown in Fig. 6a, when Ag loading was increased from 0 to 5 wt%, the maximal removal efficiency was achieved at 2 wt% Ag loading,

while, there was no apparent improvement with the increase of the Ag content. This implies that 2 wt% of Ag could absorb all the light in the system. The effect of different TiO_2 loadings (0-1 wt%) on the degradation efficiency was also studied (Fig. 6b). Removal efficiency of dyes was increased with the amount of TiO_2 and the highest degradation efficiency was obtained for 0.5 wt%. It could be inferred from aforementioned discussion that most efficient catalyst was obtained at 2 wt% Ag and 0.5 wt% TiO_2 loading in this study. Therefore photocatalytic efficiency of TiO_2 was significantly enhanced by AgNPs, moreover, the bandgap of TiO_2 and recombination frequency of electron-hole pairs were reduced. Consequently, the PAN/Ag/TiO_2 NF photocatalysts could degrade pollutants with higher removal efficiency than pure PAN/TiO_2 NF under irradiation above 400 nm. Remarkably, pH has played a critical role in the photocatalytic reaction. From Fig. 6c, the lower pH conditions corresponded to the higher degradation efficiency. Thus acidic condition was more favorable in the generation of various radical intermediates ($\bullet OH$,$\bullet O_2^-$, etc.) required for degradation of dyes. Whereas, a high concentration of oxygen strongly favors the degradation of the pollutants via formation of the active radicals (Fig. 6d). Under low oxygen concentration methyl orange, rhodamine B and methylene blue removal was only 19.0%, 22.0% and 10.0% respectively, which was mainly due to the absorption effect of the composite nanofibers. However, in the presence of oxygen, the removal efficiency of methyl orange, rhodamine B and methylene blue were reached about 99.5%, 92.0% and 99.0%, respectively.

Experiments were also carried out directly on the surface of PAN/Ag/TiO_2

nanofibers stained by the methyl orange, rhodamine B and methylene blue, and then put them under the lamp. As shown in Fig. 7, the color stains gradually disappeared according to the irradiation time. In 20 min irradiation, the methyl orange was completely degraded on the PAN/Ag/TiO_2 composite nanofibers and about 120 min was needed for rhodamine B and methylene blue, which was depended on the pollutants chemical structures and properties. This demonstrated that the Ag/TiO_2 composite nanofibers have excellent property of self-cleaning under irradiation.

3.5 Possible photodegradation mechanism

In order to explore possible photodegradation mechanism, active species trapping experiments were carried out by using different individual radical scavengers. Particularly BQ, TBA and EDTA were used as •O_2-, •OH, h^+ scavengers, respectively. From Fig. 8, the photodegradation of dyes were apparently inhibited in the presence of trapping agents. The addition of BQ and TBA indicated that •O_2- and •OH played dominant roles in the photocatalytic degradation of dyes.

On the basis of these experimental results, the possible photocatalytic degradation mechanism of dyes on the Ag/TiO_2 NF was proposed, as shown in Fig. 9. Electrons accumulated at AgNPs or the conduction band of TiO_2 can be transferred to oxygen molecules adsorbed on the surface to form free oxygen radicals, such as •O_2^-, •HO_2, •OH, and so forth, while the photo induced holes were apt to react with surface-bound H_2O or OH^- to produce the hydroxyl radical species which were potentially strong oxidant for the mineralization of organic pollutants. The following equations (Eqs. (1) - (8) summarize the main photocatalytic process.

$Ag/TiO_2 + h\nu \rightarrow Ag/TiO_2 (h^+ + e^-)$ (1)

$h^+ + H_2O \rightarrow \bullet OH + H^+$ (2)

$O_2 + e^- \rightarrow \bullet O_2^-$ (3)

$\bullet O_2^- + \text{dye} \rightarrow \text{dye decoloration} + H_2O$ (4)

$\bullet O_2^- + H_2O \rightarrow \bullet HO_2 + OH^-$ (5)

$\bullet HO_2 + H_2O \rightarrow H_2O_2 + \bullet OH$ (6)

$H_2O_2 \rightarrow \bullet OH$ (7)

$\bullet OH + \text{dye} \rightarrow \text{dye decoloration} + H_2O$ (8)

3.6. Antibacterial properties of Ag/TiO_2 nanofibers

The antibacterial properties of electrospun PAN/Ag/TiO_2 nanofibers against *E. coli* and *S. aureus* were tested using the agar plate method. As for the pure PAN fiber mats, no inhibition zones were observed against both types of bacteria, this was in line with the non-bactericidal property of PAN materials. Remarkably, inhibition zones were clearly observed for all of the Ag and Ag/TiO_2 containing specimens (Fig. 10 A1, B1) and the inhibition zones of Ag/TiO_2 samples were larger than that of the Ag containing materials. The results showed that superior properties and synergistic antibacterial effects against *S. aureus* and *E. coli* could be obtained by a combination of Ag with TiO_2. Fig. 10 (A2, B2) is depicting the morphology of the bacterial cells interacted with the PAN/Ag/TiO_2 nanofiber mats and the inactivated cells exhibited membranes that appeared wrinkled and lost their cellular integrity, which indicates that bacteria have experienced irreversible cell damage and cell death. Fig. 10C shows the bactericidal kinetics of the PAN/Ag/TiO_2 hybrid nanofiber mats, which exhibited

efficient antibacterial activity i.e. 95% of *E. coli* and 99% of *S. aureus* were killed within 2 h. Kim et al. [38] have suggested that the antimicrobial activity of AgNPs may have resulted from the formation of free radicals and the subsequent free radical-induced membrane damage. The irregularly shaped pits in the outer cell membrane were resulted from the metal depletion. This alters the permeability of the membrane and allowed for lipopolysaccharide molecules and membrane proteins to be released [39]. Due to the high surface area-to-volume ratios of the AgNPs, there was an abundance of silver atoms available on the surface of the nanoparticles, which was speculated to be the main factors of the cell membrane disruption.

4. Conclusions

High throughput of PAN based Ag/TiO_2 composite nanofibers was prepared by a one-step needleless electrospinning method. The needless electrospinning method apparently improved the production of nanofibers, which could yield over 1.4 kg/d of nanofibers. The addition of $AgNO_3$ significantly improved the conductivity of the spinning solution which was positive for the formation of nanofibers. This method features the novelty of using electrospinning solvent (DMF) as the reducing agent for the in situ formation of AgNPs. The obtained $PAN/Ag/TiO_2$ composite nanofibers exhibited excellent photocatalytic activity for the decomposition of organic pollutants under irradiation above 400 nm. The degradation efficiency of methyl orange, rhodamine B and methylene blue were 99.5%, 92% and 99%, respectively. The $\bullet O_2^-$ and •OH played dominant roles in the photocatalytic degradation of dyes. The composite mats exhibited strong antibacterial activities, e.g. 95% of *E. coli* and 99%

of *S. aureus* were killed within 2 h. High antibacterial activity was ascribed to the AgNPs with large surface area could help to increase the interaction opportunity with the bacterial surface and promoted antibacterial effect. These multifunctional PAN/Ag/TiO_2 composite nanofibers have excellent water durability due to the hydrophobic property of PAN and they can be recovered and reused for wastewater treatment. This one-step synthesized composite nanofiber mat can become an eco-friendly and cost effective pollutants treatment media. In addition, our findings may open a new gateways for facile fabrication of various stabilized composite photocatalysts with more diverse applications in biomedical, environmental remediation, sensitization and solar energy fields.

Acknowledgements

This work was supported by the National Key R&D Program of China (2017YFA0207203), National Natural Science Foundation of China (21407160, 21107055), Natural Science Funds Fund from Tianjin (13JCYBJC20300) and Strategic Priority Research Program of the Chinese Academy of Sciences (XDA09030203).

References

[1] A. Fujishima, K. Honda, Electrochemical photolysis of water at a semiconductor electrode, Nature, 238 (1972) 37-38.

[2] M.R. Hoffmann, S.T. Martin, W.Y. Choi, D.W. Bahnemann, Environmental applications of semiconductor photocatalysis Chem. Rev., 95 (1995) 69-96.

[3] C. Hu, Y.C. Tang, J.C. Yu, P.K. Wong, Photocatalytic degradation of cationic blue X-GRL adsorbed on TiO_2/SiO_2 photocatalyst, Appl. Catal. B: Environ., 40 (2003) 131-140.

[4] A. Ayati, A. Ahmadpour, F.F. Bamoharram, B. Tanhaei, M. Manttari, M. Sillanpaa, A review on catalytic applications of Au/TiO_2 nanoparticles in the removal of water pollutant, Chemosphere, 107 (2014) 163-174.

[5] A. Kudo, Y. Miseki, Heterogeneous photocatalyst materials for water splitting, Chem. Soc. Rev., 38

(2009) 253-278.
[6] P.F. Fu, Y. Luan, X.G. Dai, Preparation of activated carbon fibers supported TiO_2 photocatalyst and evaluation of its photocatalytic reactivity, J. Mol. Catal. A-Chem., 221 (2004) 81-88.
[7] L.W. Zhang, H.B. Fu, Y.F. Zhu, Efficient TiO_2 photocatalysts from surface hybridization of TiO_2 particles with graphite-like carbon, Adv. Funct. Mater., 18 (2008) 2180-2189.
[8] W.Y. Choi, A. Termin, M.R. Hoffmann, The role of metal-ion dopants in quantum-sized TiO_2 correlation between photoreactivity and charge carrier recombination dynamics, J. Phys. Chem., 98 (1994) 13669-13679.
[9] S. Ikeda, N. Sugiyama, B. Pal, G. Marci, L. Palmisano, H. Noguchi, K. Uosaki, B. Ohtani, Photocatalytic activity of transition-metal-loaded titanium(IV) oxide powders suspended in aqueous solutions: Correlation with electron-hole recombination kinetics, Phys. Chem. Chem. Phys., 3 (2001) 267-273.
[10] H. Park, W. Choi, Effects of TiO_2 surface fluorination on photocatalytic reactions and photoelectrochemical behaviors, J. Phys. Chem. B, 108 (2004) 4086-4093.
[11] R. Kaur, B. Pal, Size and shape dependent attachments of Au nanostructures to TiO_2 for optimum reactivity of Au-TiO_2 photocatalysis, J. Mol. Catal. A-Chem., 355 (2012) 39-43.
[12] X.D. Wang, R.A. Caruso, Enhancing photocatalytic activity of titania materials by using porous structures and the addition of gold nanoparticles, J. Mater. Chem., 21 (2011) 20-28.
[13] S.G. Kumar, L.G. Devi, Review on modified TiO_2 photocatalysis under UV/visible light: selected results and related mechanisms on interfacial charge carrier transfer dynamics, J. Phys. Chem. A, 115 (2011) 13211-13241.
[14] K.D. Kim, D.N. Han, J.B. Lee, H.T. Kim, Formation and characterization of Ag-deposited TiO_2 nanoparticles by chemical reduction method, Scripta Mater., 54 (2006) 143-146.
[15] M.K. Seery, R. George, P. Floris, S.C. Pillai, Silver doped titanium dioxide nanomaterials for enhanced visible light photocatalysis, J. Photoch. Photobio. A., 189 (2007) 258-263.
[16] K. Page, R.G. Palgrave, I.P. Parkin, M. Wilson, S.L.P. Savin, A.V. Chadwick, Titania and silver-titania composite films on glass-potent antimicrobial coatings, J. Mater. Chem., 17 (2007) 95-104.
[17] H.J. Zhang, G.H. Chen, Potent antibacterial activities of Ag/TiO_2 nanocomposite powders synthesized by a one-pot sol-gel method, Environ. Sci. Technol., 43 (2009) 2905-2910.
[18] G. Wang, Q. Wang, W. Lu, J.H. Li, Photoelectrochemical study on charge transfer properties of TiO_2-B nanowires with an application as humidity sensors, J. Phys. Chem. B, 110 (2006) 22029-22034.
[19] L.B. Yang, X. Jiang, W.D. Ruan, J.X. Yang, B. Zhao, W.Q. Xu, J.R. Lombardi, Charge transfer induced surface enhanced raman scattering on Ag-TiO_2 nanocomposites, J. Phys. Chem. C 113 (2009) 16226-16231.
[20] H. Dong, D. Wang, G. Sun, J.P. Hinestroza, Assembly of metal nanoparticles on electrospun nylon 6 nanofibers by control of interfacial hydrogen-bonding interactions, Chem. Mater., 20 (2008) 6627-6632.
[21] L.W. Ji, Z. Lin, A.J. Medford, X.W. Zhang, In-situ encapsulation of nickel particles in electrospun carbon nanofibers and the resultant electrochemical performance, Chem. Eur. J., 15 (2009) 10718-10722.
[22] H.R. Pant, D.R. Pandeya, K.T. Nam, W.I. Baek, S.T. Hong, H.Y. Kim, Photocatalytic and antibacterial properties of a TiO_2/nylon-6 electrospun nanocomposite mat containing silver nanoparticles, J. Hazard. Mater., 189 (2011) 465-471.
[23] J.W. Xie, X.R. Li, Y.N. Xia, Putting electrospun nanofibers to work for biomedical research,

Macromol. Rapid Comm., 29 (2008) 1775-1792.
[24] H.B. Deng, X.Y. Li, B. Ding, Y.M. Du, G.X. Li, J.H. Yang, X.W. Hu, Fabrication of polymer/layered silicate intercalated nanofibrous mats and their bacterial inhibition activity, Carbohyd. Polym., 83 (2011) 973-978.
[25] H.B. Deng, P.H. Lin, W. Li, S.J. Xin, X. Zhou, J.H. Yang, Hydroxypropyl chitosan/organic rectorite-based nanofibrous mats with intercalated structure for bacterial inhibition, J. Biomat. Sci-Polyme. E., 24 (2013) 485-496.
[26] Y.R. Dai, J.F. Niu, L.F. Yin, J.J. Xu, K. Sun, Enhanced sorption of perfluorooctane sulfonate (PFOS) on carbon nanotube-filled electrospun nanofibrous membranes, Chemosphere, 93 (2013) 1593-1599.
[27] M.J. Nalbandian, M.L. Zhang, J. Sanchez, S. Kim, Y.H. Choa, D.M. Cwiertny, N.V. Myung, Synthesis and optimization of Ag-TiO_2 composite nanofibers for photocatalytic treatment of impaired water sources, J. Hazard. Mater., 299 (2015) 141-148.
[28] A. Veres, T. Rica, L. Janovak, M. Domok, N. Buzas, V. Zollmer, T. Seemann, A. Richardt, I. Dekany, Silver and gold modified plasmonic TiO_2 hybrid films for photocatalytic decomposition of ethanol under visible light, Catal. Today, 181 (2012) 156-162.
[29] J. Ali, N. Ali, S.U.U. Jamil, H. Waseem, K. Khan, G. Pan, Insight into eco-friendly fabrication of silver nanoparticles by Pseudomonas aeruginosa and its potential impacts, J. Environ. Chem. Eng., 5 (2017) 3266-3272.
[30] M.Q. Liu, J. Zhao, C.F. Xiao, Q. Quan, X.F. Li, PPy-assisted fabrication of Ag/TiO_2 visible-light photocatalyst and its immobilization on PAN fiber, Mater. Design, 104 (2016) 428-435.
[31] A. Amarjargal, L.D. Tijing, M.T.G. Ruelo, D.H. Lee, C.S. Kim, Facile synthesis and immobilization of Ag-TiO_2 nanoparticles on electrospun PU nanofibers by polyol technique and simple immersion, Mater. Chem. Phys., 135 (2012) 277-281.
[32] A. Abdolmaleki, S. Mallakpour, S. Borandeh, In situ synthesis of silver nanoparticles in novel L-phenylalanine based poly(amide-benzimidazole-imide) matrix through metal complexation method using N,N '-dimethylformamide as a reaction medium and reducing agent, Polym. Plast. Technol., 54 (2015) 1002-1008.
[33] L. Wang, C. Zhang, F. Gao, G. Pan, Needleless electrospinning for scaled-up production of ultrafine chitosan hybrid nanofibers used for air filtration, Rsc Adv., 6 (2016) 105988-105995.
[34] L. Wang, C. Zhang, F. Gao, G. Mailhot, G. Pan, Algae decorated TiO_2/Ag hybrid nanofiber membrane with enhanced photocatalytic activity for Cr(VI) removal under visible light, Chem. Eng. J., 314 (2017) 622-630.
[35] P. Wang, B. Huang, X. Qin, X. Zhang, Y. Dai, J. Wei, M.-H. Whangbo, Ag@AgCl: A highly efficient and stable photocatalyst active under visible light, Angew. Chem. Int. Ed., 47 (2008) 7931-7933.
[36] J. Ali, A. Hameed, S. Ahmed, M.I. Ali, S. Zainab, N. Ali, Role of catalytic protein and stabilising agents in the transformation of Ag ions to nanoparticles by Pseudomonas aeruginosa, Iet Nanobiotechnol., 10 (2016) 295-300.
[37] J.H. He, I. Ichinose, T. Kunitake, A. Nakao, Y. Shiraishi, N. Toshima, Facile fabrication of Ag-Pd bimetallic nanoparticles in ultrathin TiO_2-gel films: Nanoparticle morphology and catalytic activity, J. Am. Chem. Soc., 125 (2003) 11034-11040.
[38] J.S. Kim, E. Kuk, K.N. Yu, J.H. Kim, S.J. Park, H.J. Lee, S.H. Kim, Y.K. Park, Y.H. Park, C.Y. Hwang, Y.K. Kim, Y.S. Lee, D.H. Jeong, M.H. Cho, Antimicrobial effects of silver nanoparticles, Nanomed. Nanotechnol., 3 (2007) 95-101.
[39] A. Ogar, G. Tylko, K. Turnau, Antifungal properties of silver nanoparticles against indoor mould

growth, Sci. Total Environ., 521 (2015) 305-314.

Figure captions

Fig. 1. (a) Fe-SEM image of Ag/TiO_2 composite nanofibers, (b) diameter distribution of nanofibers, (c) TEM image of nanofibers, and (d) EDX spectra of composite nanofibers.

Fig. 2. XRD spectra for different nanofiber mats (a) PAN, (b) PAN/TiO_2 and (c) $PAN/Ag/TiO_2$

Fig. 3. Absorption spectra of composite thin films modified with TiO_2 and Ag nanoparticles.

Fig. 4. Photocatalytic degradation of dye pollutants under different conditions. The initial concentration of dyes and composite nanofibers were 10 ppm and 50 ppm, respectively.

Fig. 5. Absorbance of dyes solution according to the irradiation time. The initial concentration of dyes and $PAN/Ag/TiO_2$ composite nanofibers were 10 ppm and 50 ppm, respectively.

Fig. 6. Effect of different parameters on the degradation efficiency: (a) $AgNO_3$ loading, (b) TiO_2 loading, (c) initial solution pH and (d) oxygen. The initial concentration of dyes and composite nanofibers were 10 ppm and 50 ppm, respectively.

Fig. 7. Images of PAN/Ag/TiO_2 nanofiber samples stained with different dyes: (a) methyl orange, (b) rhodamine B and (c) methylene blue under the irradiation of metal halide lamp according to the reaction time.

Fig. 8. Influence of different trapping agents on the photodegradation of dyes

Fig. 9. Schematic diagram of photocatalytic degradation mechanism

Fig. 10. The inhibition zone of various nanofiber mats (a) PAN, (b) PAN/Ag and (c) PAN/Ag/TiO_2 against (A1) *S. aureus* and (B1) *E. coli*; SEM images of *S. aureus* (A2) and *E. coli* (B2) in contact with PAN/Ag/TiO_2 nanofiber mats; (C) The bactericidal activity of PAN/Ag/TiO_2 composite nanofibers.

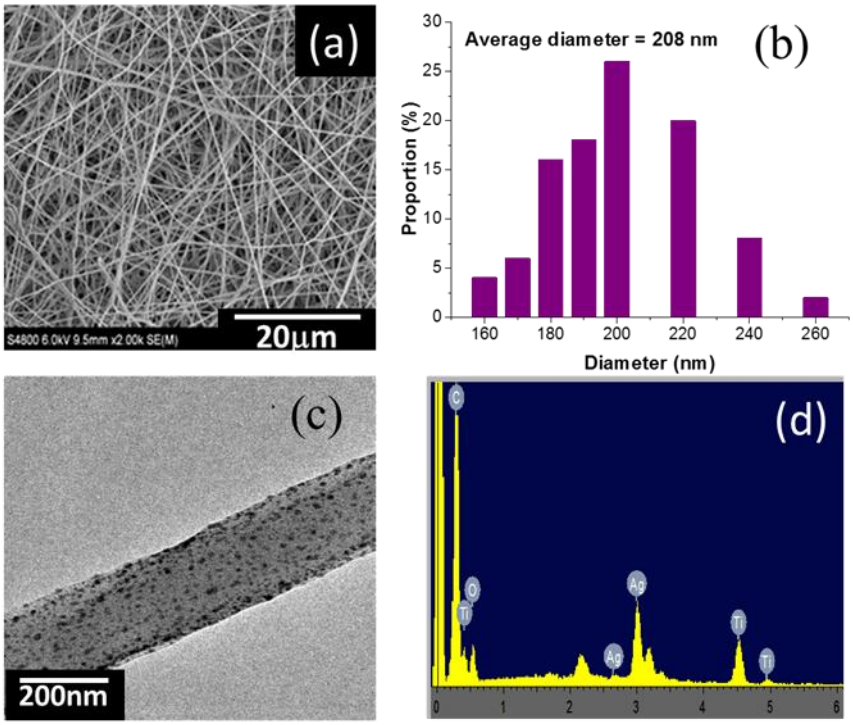

Fig. 1. (a) Fe-SEM image of Ag/TiO_2 composite nanofibers, (b) diameter distribution of nanofibers, (c) TEM image of nanofibers, and (d) EDX spectra of composite

nanofibers.

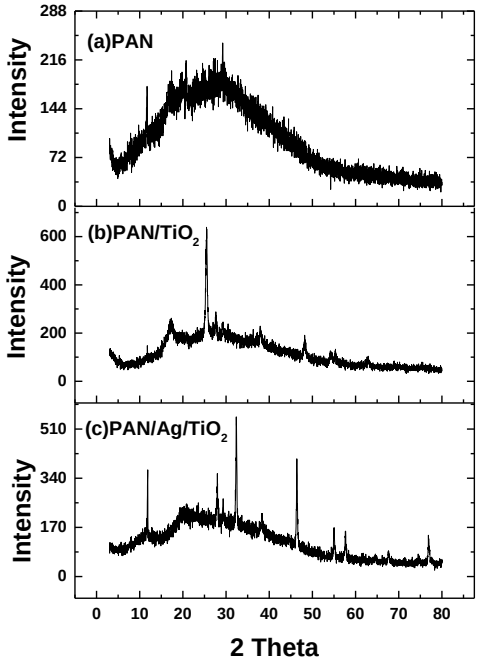

Fig. 2. XRD spectra for different nanofiber mats (a) PAN, (b) PAN/TiO_2 and (c) PAN/Ag/TiO_2

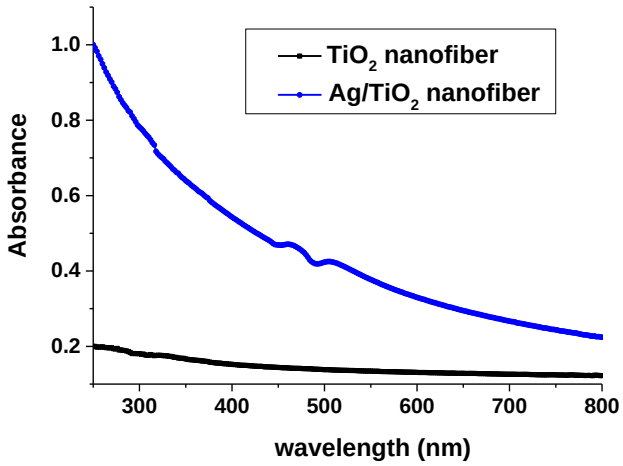

Fig. 3. Absorption spectra of composite thin films modified with TiO_2 and Ag nanoparticles.

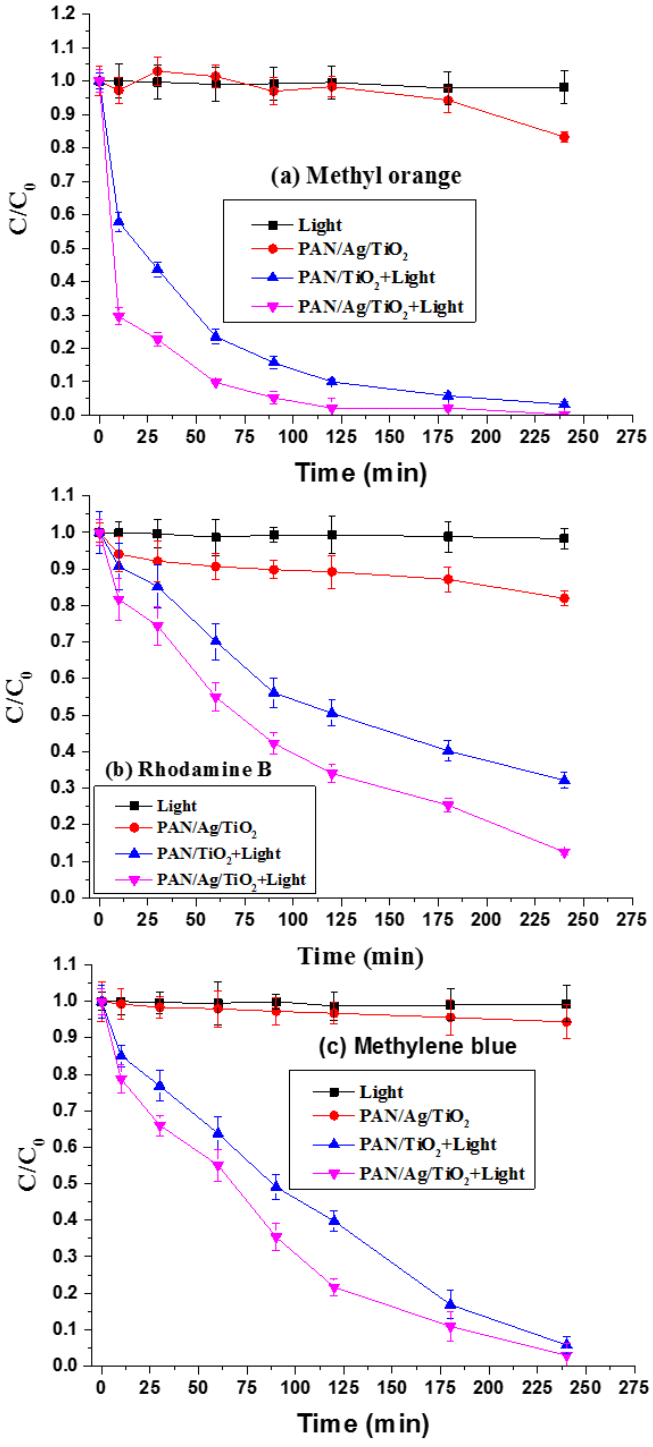

Fig. 4. Photocatalytic degradation of dye pollutants under different conditions. The initial concentration of dyes and composite nanofibers were 10 ppm and 50 ppm, respectively.

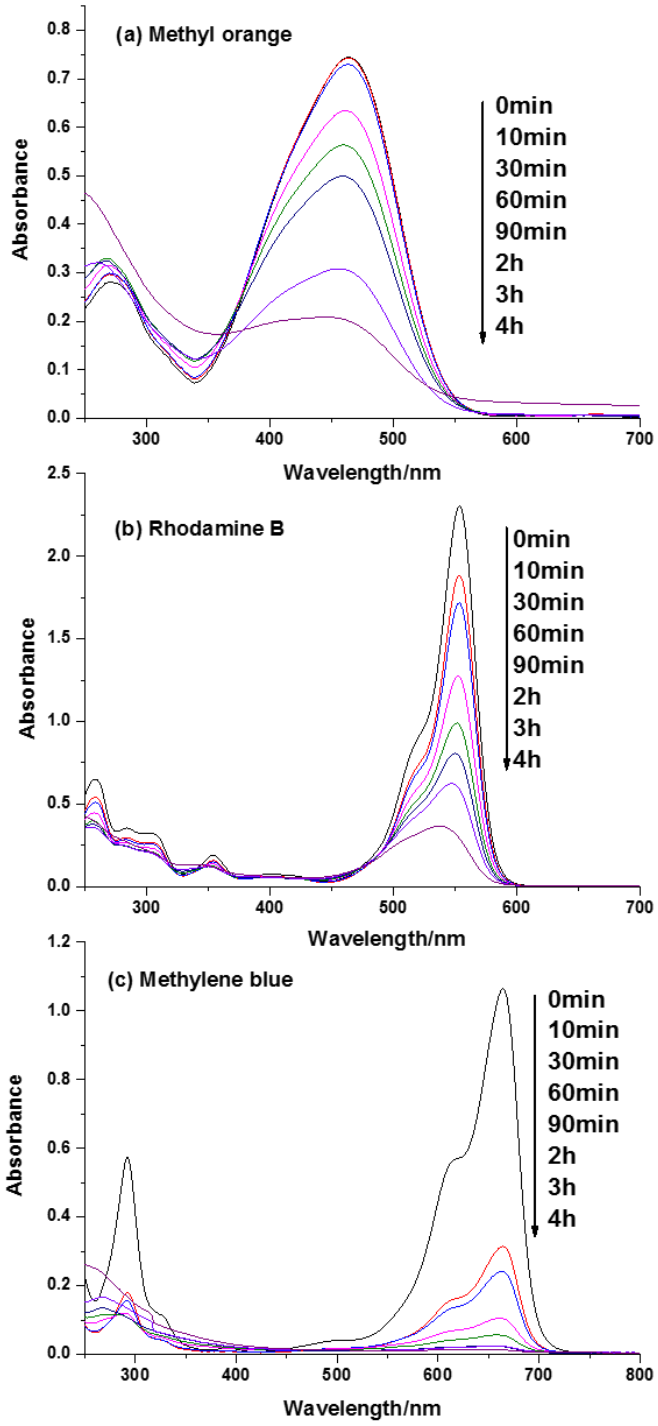

Fig. 5. Absorbance of dyes solution according to the irradiation time. The initial concentration of dyes and PAN/Ag/TiO_2 composite nanofibers were 10 ppm and 50 ppm, respectively.

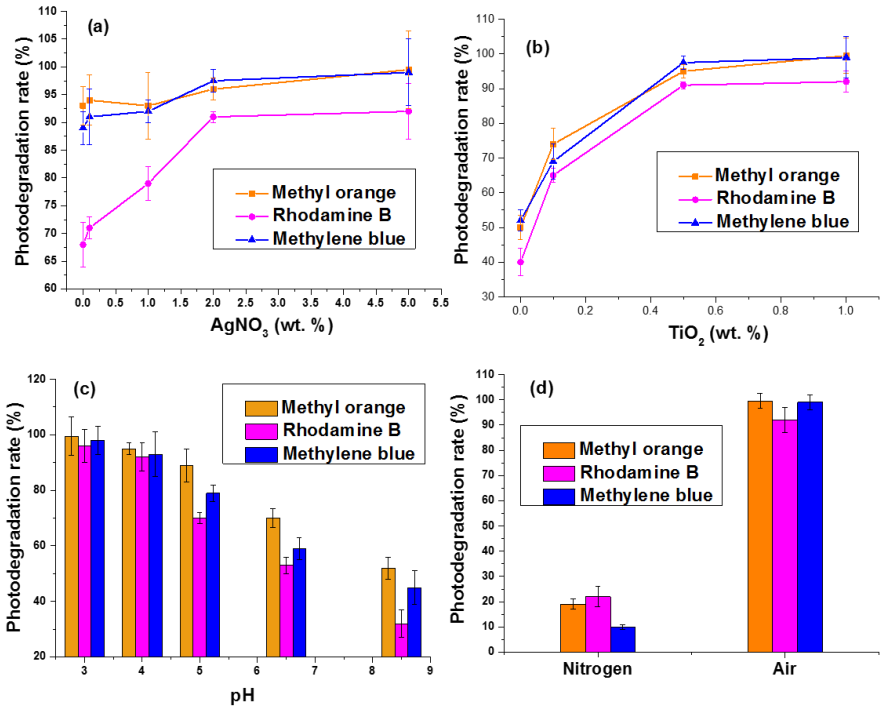

Fig. 6. Effect of different parameters on the degradation efficiency: (a) $AgNO_3$ loading, (b) TiO_2 loading, (c) initial solution pH and (d) oxygen. The initial concentration of dyes and composite nanofibers were 10 ppm and 50 ppm, respectively.

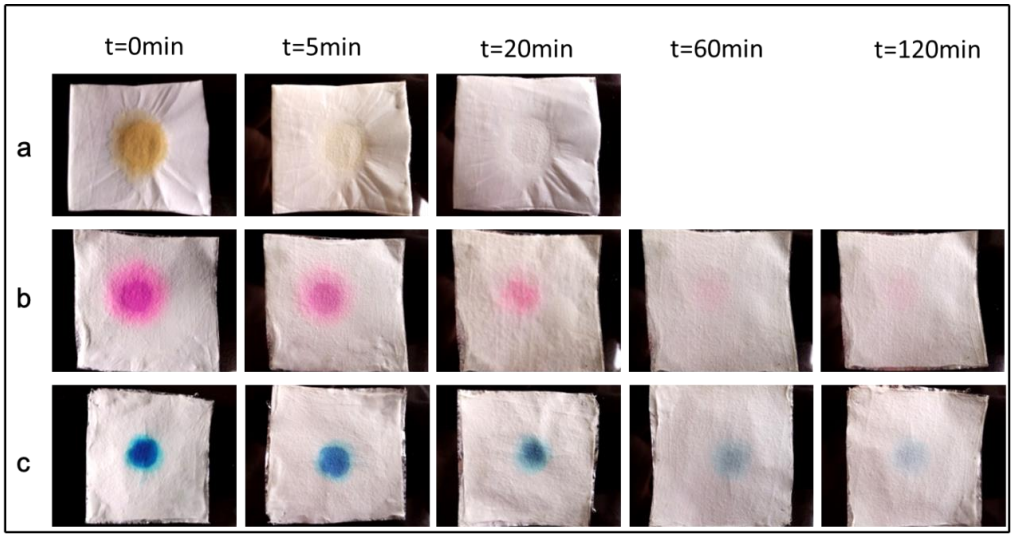

Fig. 7. Images of PAN/Ag/TiO_2 nanofiber samples stained with different dyes: (a) methyl orange, (b) rhodamine B and (c) methylene blue under the irradiation of metal halide lamp according to the reaction time.

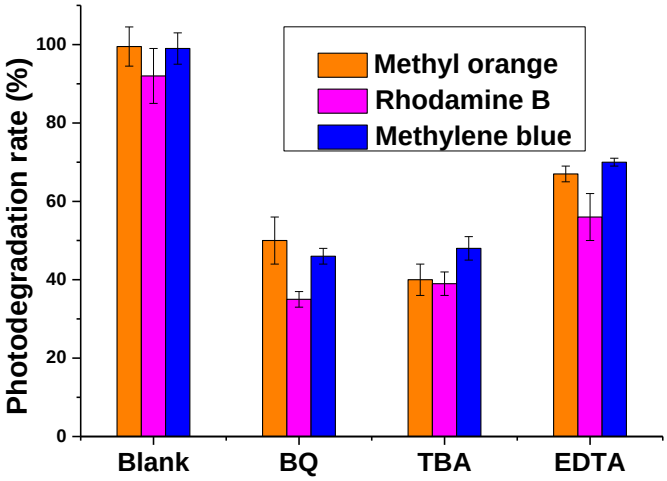

Fig. 8. Influence of different trapping agents on the photodegradation of dyes

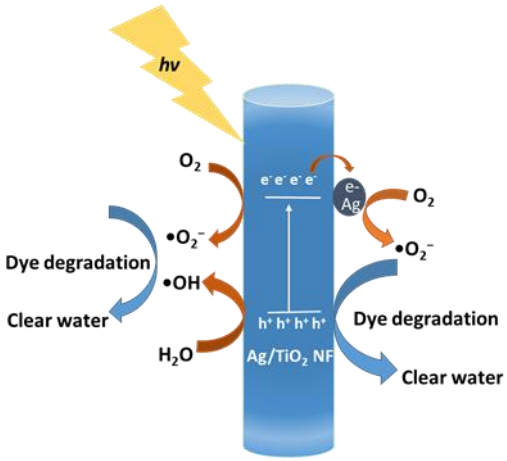

Fig. 9. Schematic diagram of photocatalytic degradation mechanism

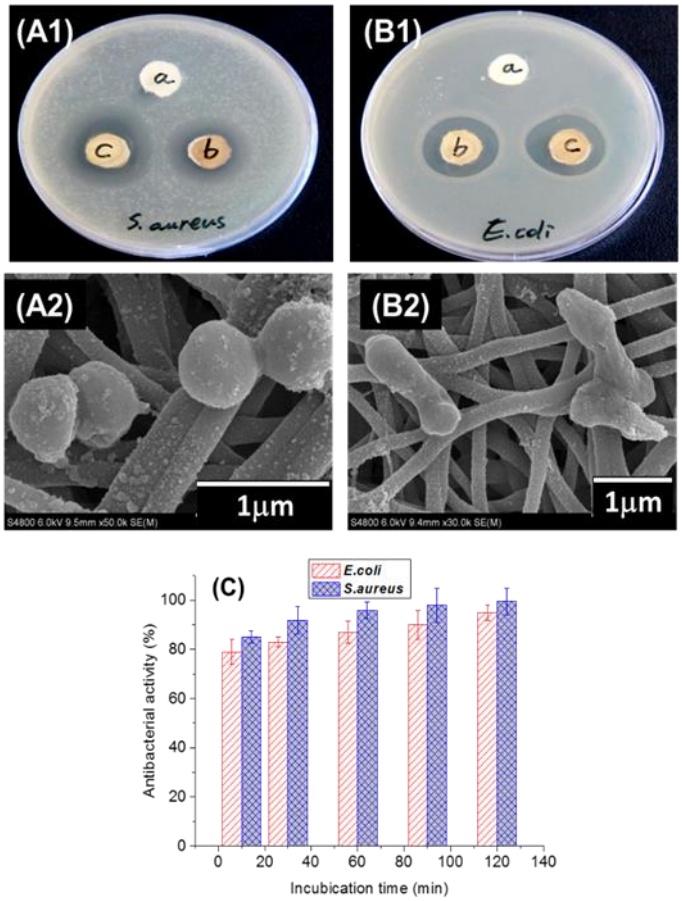

Fig. 10. The inhibition zone of various nanofiber mats (a) PAN, (b) PAN/Ag and (c) PAN/Ag/TiO_2 against (A1) *S. aureus* and (B1) *E. coli*; SEM images of *S. aureus* (A2) and *E. coli* (B2) in contact with PAN/Ag/TiO_2 nanofiber mats; (C) The bactericidal activity of PAN/Ag/TiO_2 composite nanofibers.

Table

Table 1 Effects of TiO_2 and $AgNO_3$ concentration on the nanofiber diameters of PAN/Ag/TiO_2 composite nanofibers

PAN 10%	TiO_2 (%)	σ(mS/cm)	d_{ave} (nm)
2%Ag	0	1.103	162
	0.1	1.105	170
	0.5	1.115	213
	1.0	1.152	243
PAN 10%	Ag (%)		
0.5%TiO_2	0	0.119	261
	0.1	0.213	240
	1.0	0.725	238
	2.0	1.115	213
	5.0	1.920	202